Electronic Supplementary Material (ESI) for Inorganic Chemistry Frontiers.

Supporting Information

Adjustable composition on Self-supported Amorphous Ni-Fe-P nanosheets decorated NiP microspheres for efficient and stable overall alkaline freshwater/seawater splitting

Shi-Yu Lu[1,*], Ling Wang[2], Chunjie Wu[2], Jun Zhang[1], Wenzhao Dou[2], Tingting Hu[1], Rong Wang[1], Yin Liu[1], Qian Yang[1], Meng Jin[1,*]

[1]College of Metallurgy and Materials Engineering, Chongqing University of Science and Technology, Chongqing 401331, China.

[2]College of Chemistry and Chemical Engineering, Chongqing University of Science and Technology, Chongqing 401331, China.

*Corresponding authors Emails: lushiyu@cqust.edu.cn (S. Lu); jinmeng@cqust.edu.cn (M. Jin)

Experimental section

Reagents and Materials

Potassium hydroxide (KOH, 95%), hydrochloric acid (HCl, 37%), nickel sulfate hexahydrate ($NiSO_4·6H_2O$, analytical grade), ammonium chloride (NH_4Cl, 99.5%), sodium hypophosphite ($NaH_2PO_2·H_2O$, analytical grade), iron nitrate nonahydrateuuu ($Fe(NO_3)_3·9H_2O$, 98.5%), anhydrous ethanol (C_2H_5OH, 99%) were obtained from Macklin reagents Co., Ltd. Co. Commercial Pt/C (20%) and ruthenium oxide (RuO_2, 99.9%) were purchased from singma Co., USA. Nafion (5.0 wt%) was obtained from DuPont™. The Ni foam (NF, thickness:1 mm) was from Suzhou Wingrise Energy Technology Co, Ltd. All chemicals were used directly without any further purification.

Preparation of A-NiFeP/NiP

The A-NiFeP/NiP was fabricated by electrodeposition. NF (1 cm × 1.2 cm) was ultrasonic cleaned with alcohol and deionized water for 10 min in sequence and then dried in vacuum at 60 °C for 8 h. The electrodeposition process was carried out using the three-electrode system, the pretreated NF, saturated calomel electrode (SCE) and the platinum foils were used as working electrode, reference electrode and counter electrode, respectively. The A-NiFeP/NiP were conducted at a cathodic current density of 500 mA cm^{-2} for 300 s at room temperature. The electrolyte composition and prepared A-NiFeP/NiP names were listed in Table S1.

Table S1 Electrodeposition solution details.

Solution number	Electrolyte composition				Films name
	$NiSO_4·6H_2O$ (M)	$Fe(NO_3)_3·9H_2O$ (M)	$NaH_2PO_2·H_2O$ (M)	NH_4Cl (M)	
1	0.095	0.005	0.5	1	A-NiFeP/NiP-Fe:5%
2	0.090	0.010	0.5	1	A-NiFeP/NiP-Fe:10%
3	0.080	0.020	0.5	1	A-NiFeP/NiP-Fe:20%
4	0.075	0.025	0.5	1	A-NiFeP/NiP-Fe:25%
5	0.025	0.075	0.5	1	A-NiFeP/NiP-Fe:75%

Preparation of NiP and FeP

The NiP was also fabricated by electrodeposition. The electrodeposition solution consisted of $NiSO_4·6H_2O$ (0.1 M), NaH_2PO_2 (0.5 M) and NH_4Cl (1 M) with a current of -500 mA cm^{-2} for 300 s at room temperature. The FeP (electrodeposition solution $NiSO_4·6H_2O$ (0.1 M) was replaced with $Fe(NO_3)_3·9H_2O$ (0.1M) was prepared using the similar electrodeposition method.

Fabrication of Pt/C and RuO_2 NF

The powder catalyst was dispersed in water-ethanol solution ($V_{water}/V_{ethanol}$ = 1:1) with 5% Nafion and ultra-sonicated for 30 min. Later, the catalyst was dropped coating on the surface of NF with a mass loading of 0.5 mg cm^{-2}.

Characterization of electrocatalysts

The phase composition of all samples was investigated by X-ray diffraction (XRD, SHIMADZU 6100) with the 2θ ranges from 10^0 to 80^0 at a scanning rate of 5^0 min^{-1}. The morphology and structure of the samples were characterized by scanning electron microscopy (SEM, 7800F) and transmission electron microscopy (TEM, Talos F200S G2). The surface composition and valence of resulting materials were conducted on X-ray photoelectron spectroscopy (XPS, ESCALAB 250X), which was calibrated with the position of the C1s peak (binding energy: 284.6 eV).

Electrochemical measurement

All electrochemical measurements were carried out by using an electrochemical workstation (CHI 760E) at room temperature. The electrolyte was alkaline freshwater (1.0 M KOH) and seawater (1.0 M KOH + 0.5 M NaCl). The prepared films (1 cm × 1.2 cm) were used as the working electrode, a 1 cm × 1 cm platinum foil and a saturated calomel electrode (SCE) were used as the counter electrode and the reference electrode, respectively. All measured potentials were converted from SCE to the reversible hydrogen electrode (RHE) according to: $E_{RHE} = E_{SCE} + 0.241 + 0.059$ pH. The electrocatalytic activity of the synthesized electrode for the OER and HER were evaluated by performing linear sweep voltammetry (LSV) over the potential range of 1.0 to 1.9 V vs. RHE (for OER) and 0.0 V to -0.6 V vs. RHE (for HER). Furthermore, the Tafel slope of these samples was obtained by fitting the experimental data with the equation $\eta = a + b \log |j|$, where η is the overpotential, b is the Tafel slope, and j is the current density. The EIS was measured by frequency sweep from 10 kHz to 0.01 Hz at the overpotential of 1.3 V (vs. SCE) and the amplitude of 5 mV. A long-term durability test was performed using chronoamperometry measurements. The electrochemical active sites of different electrodes were measured by Cyclic voltametric (CV) at different scanning rates (20, 40, 60, 80, 100 mV s^{-1}) in the range of 0.42 V-0.52 V. The full electrolyzer configuration was assembled using the different NiFeP electrodes were used as cathode and anode, respectively in alkaline freshwater and seawater.

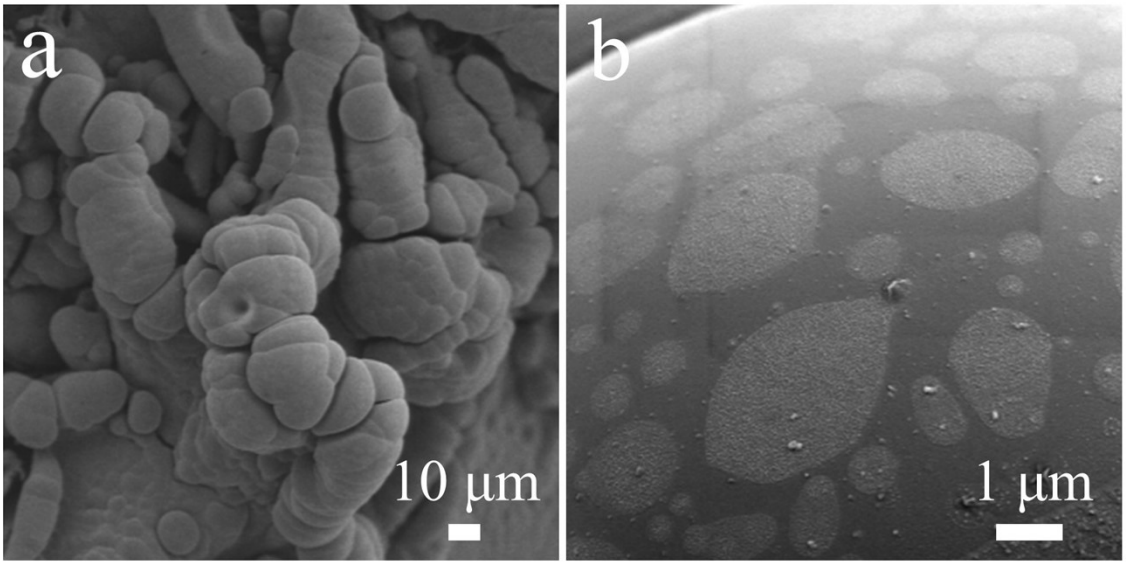

Figure S1. SEM images of A-NiFeP/NiP-Fe:5%.

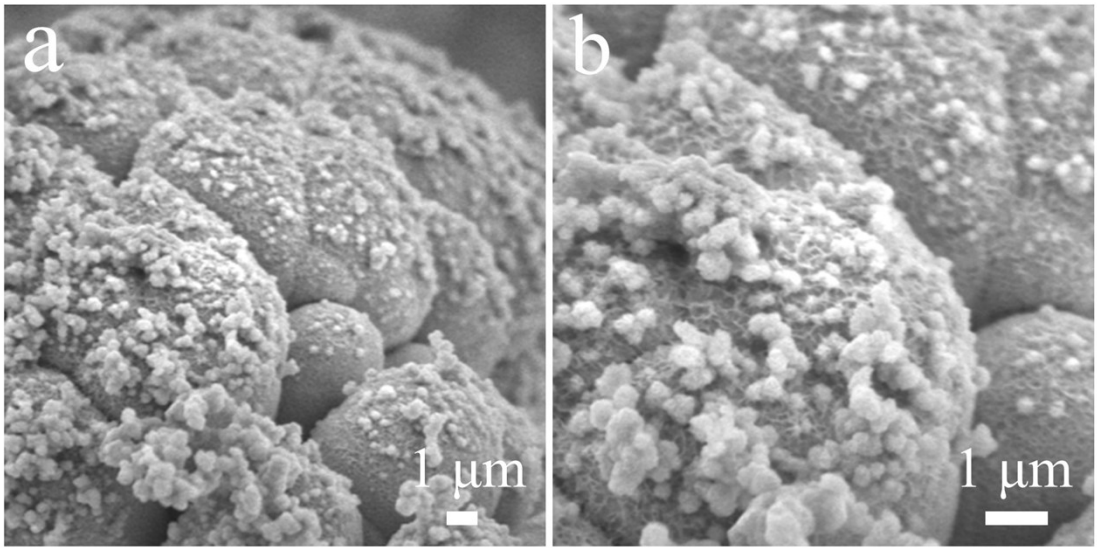

Figure S2. SEM images of A-NiFeP/NiP-Fe:20%.

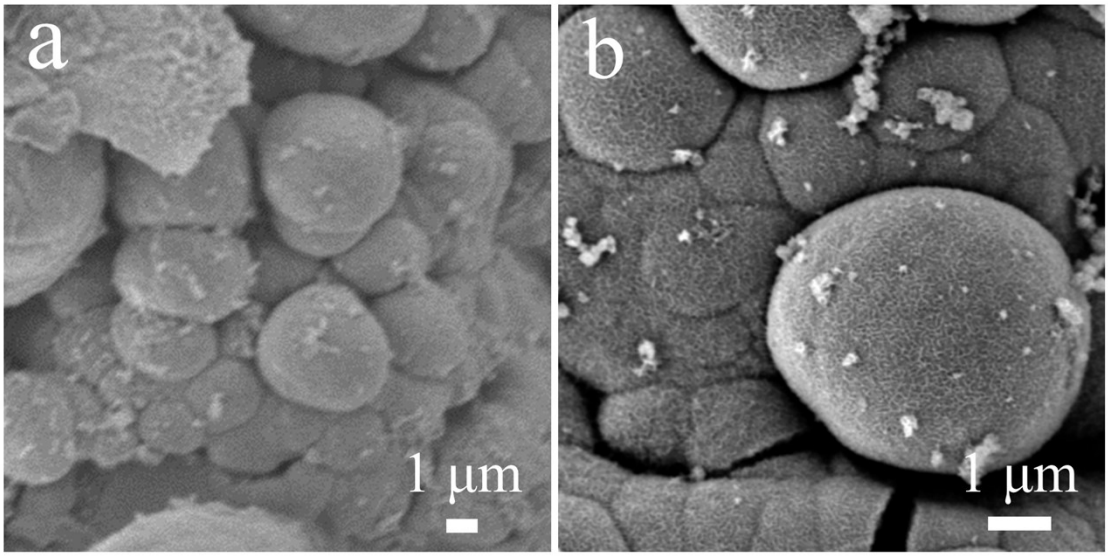

Figure S3. SEM images of A-NiFeP/NiP-Fe:75%.

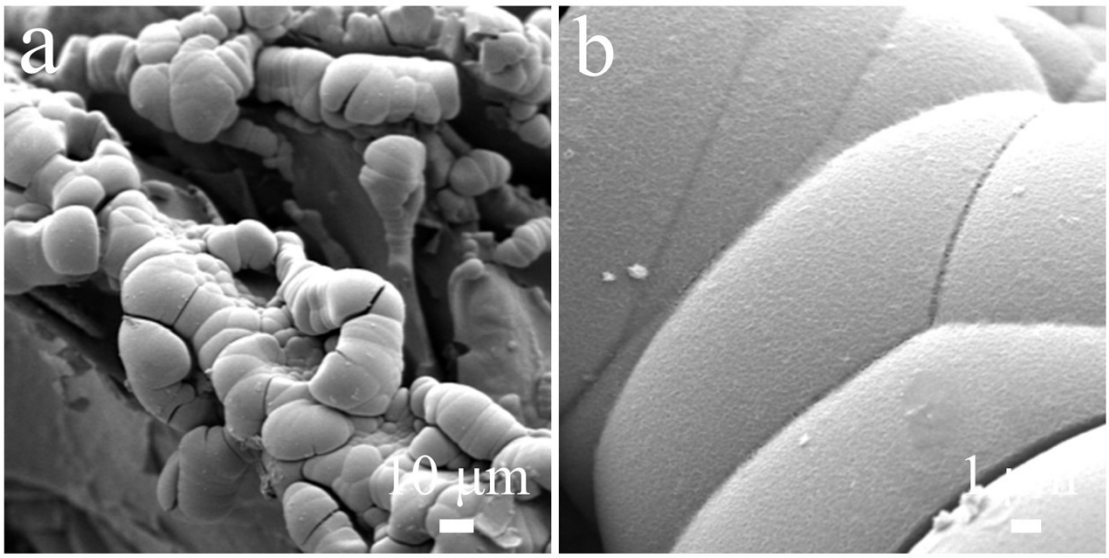

Figure S4. SEM images of NiP.

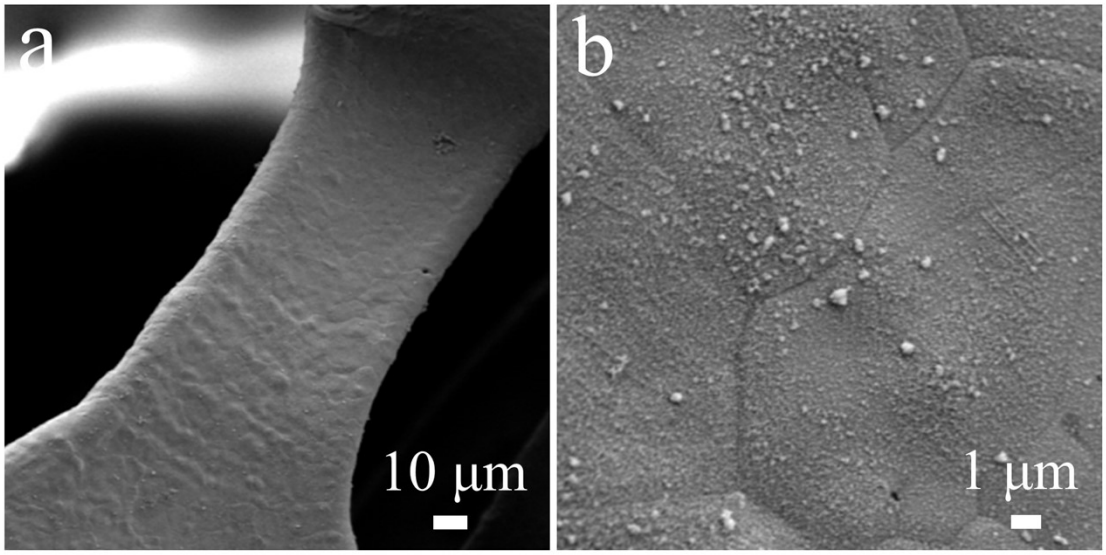

Figure S5. SEM images of FeP.

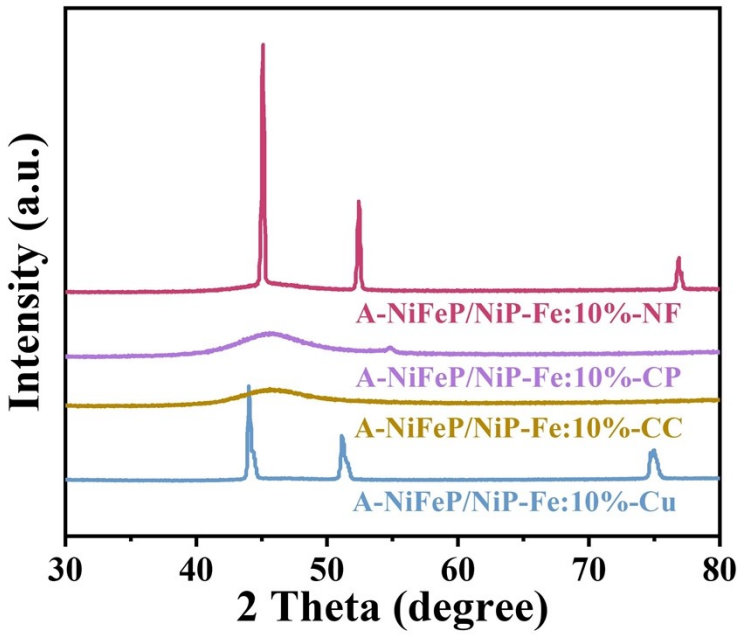

Figure S6. XRD patterns of A-NiFeP/NiP-Fe:10% on the carbon cloth, copper foam, carbon paper, nickel foam.

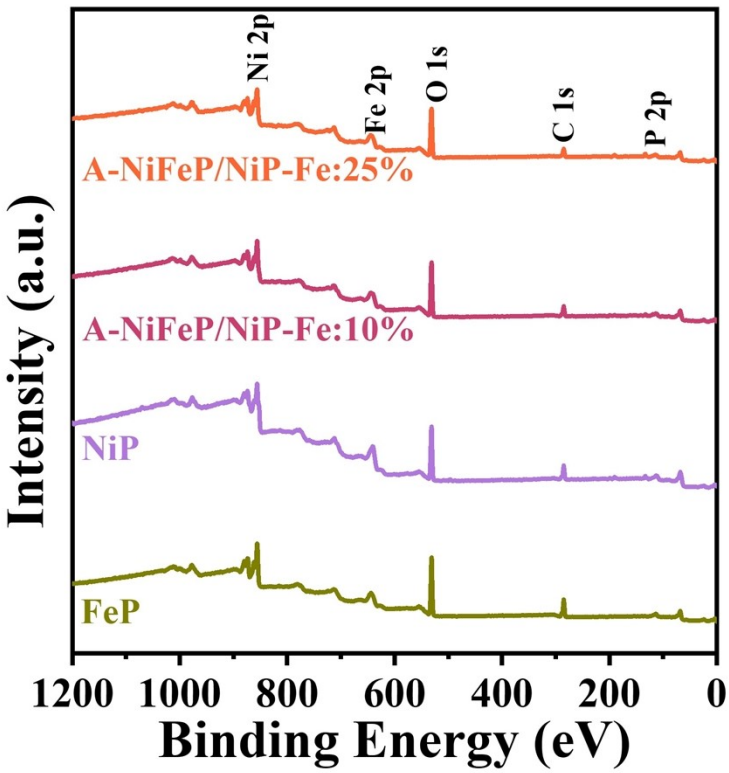

Figure S7. XPS survey spectrum of NiP, FeP, A-NiFeP/NiP-Fe:10% and A-NiFeP/NiP-Fe:25% electrocatalysts.

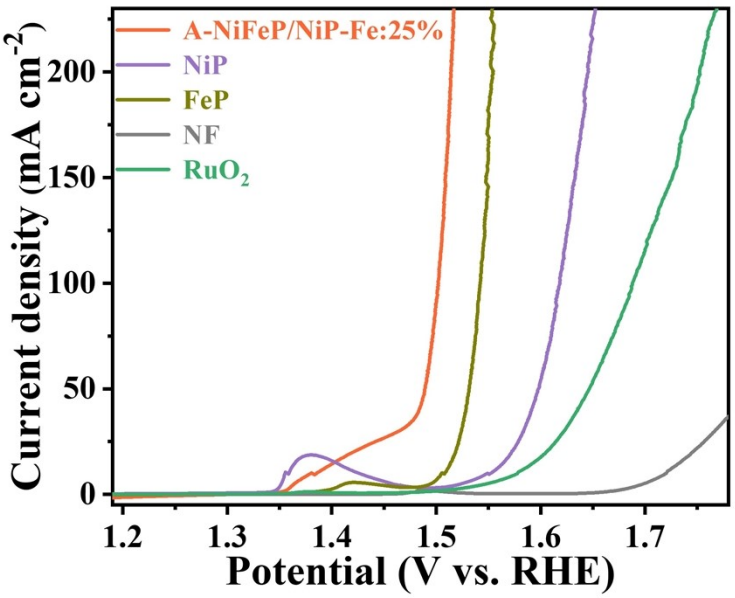

Figure S8. Polarization OER curves of NF, NiP, FeP, A-NiFeP/NiP-Fe:25% and RuO_2 electrodes in 1 M KOH.

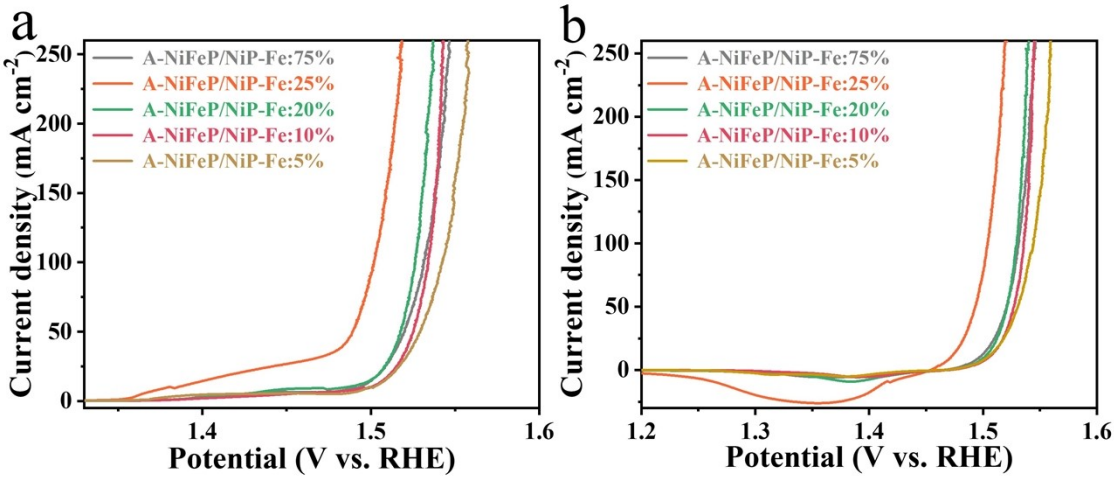

Figure S9. Polarization OER curves of A-NiFeP/NiP-Fe:5%, A-NiFeP/NiP-Fe:10%, A-NiFeP/NiP-Fe:20%, A-NiFeP/NiP-Fe:25% and A-NiFeP/NiP-Fe:75% in 1 M KOH.

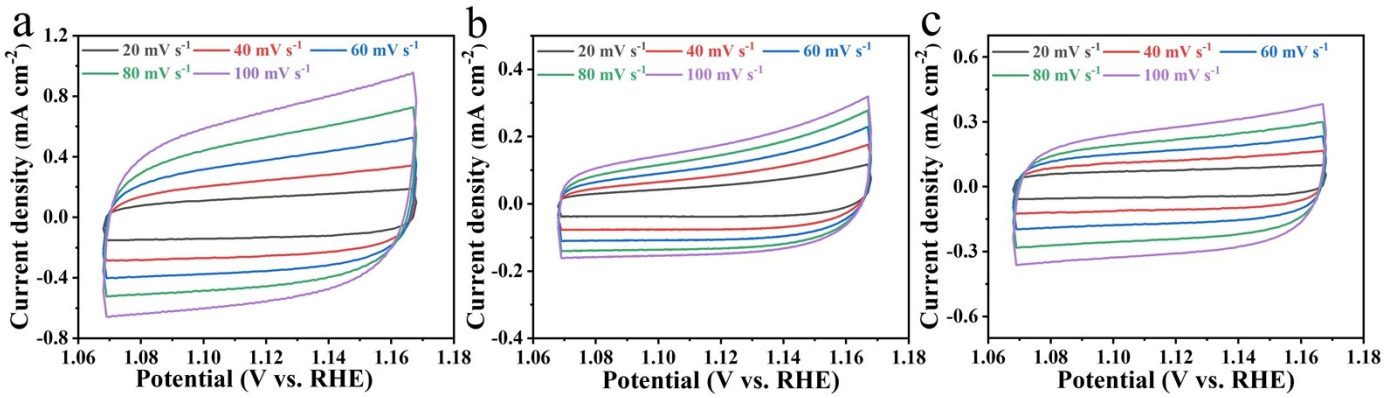

Figure S10. CV curves of (a) A-NiFeP/NiP-Fe:25%, (b) NiP and (c) FeP at different scan rate of 20, 40, 60, 80 and 100 mV s^{-1}.

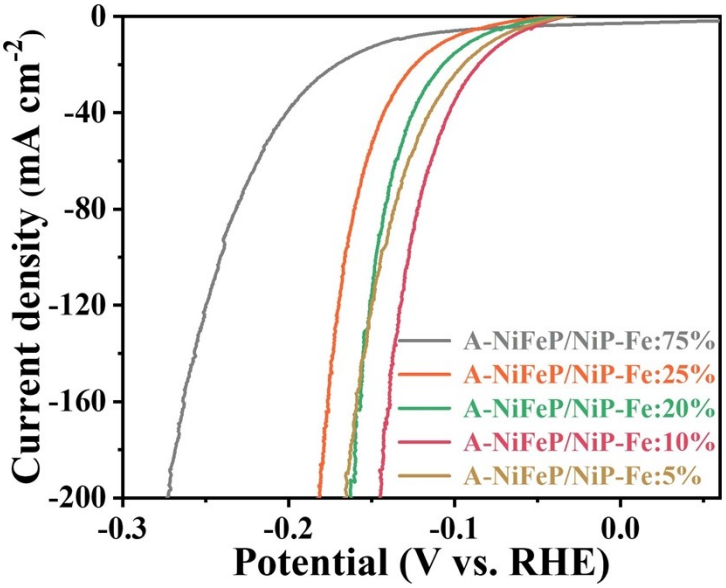

Figure S11. (a) Polarization curves of A-NiFeP/NiP-Fe:5%, A-NiFeP/NiP-Fe:10%, A-NiFeP/NiP-Fe:20%, A-NiFeP/NiP-Fe:25% and A-NiFeP/NiP-Fe:75% for HER in 1 M KOH.

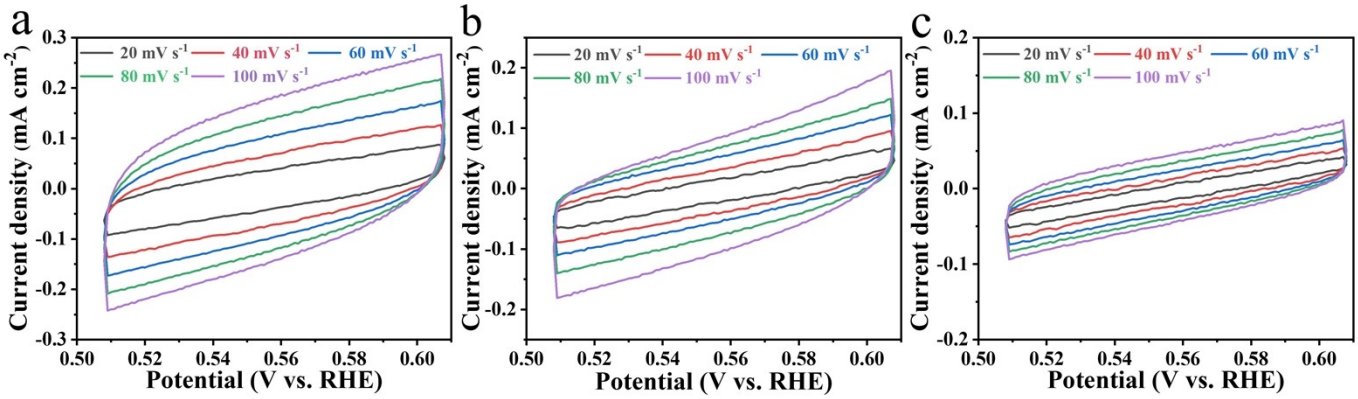

Figure S12. CV curves of (a) A-NiFeP/NiP-Fe:10%, (b) NiP and (c) FeP at different scan rate of 20, 40, 60, 80 and 100 mV s^{-1}.

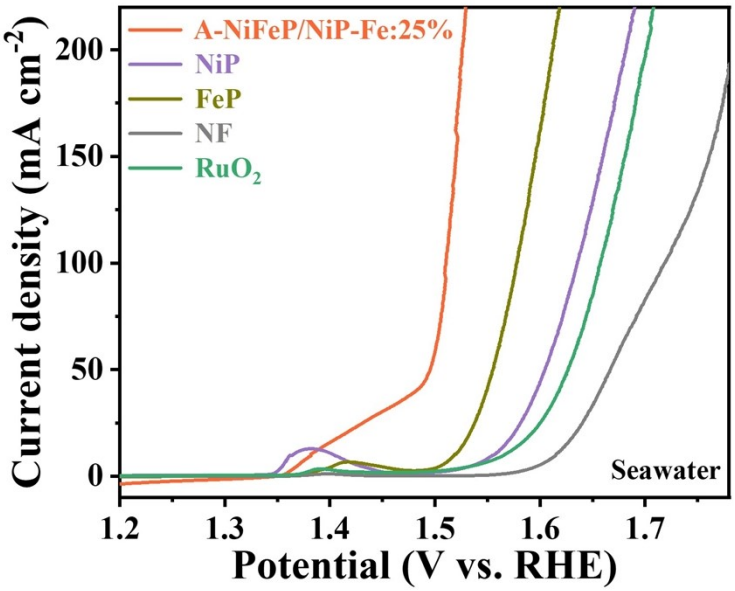

Figure S13. Polarization curves of NF, NiP, FeP, A-NiFeP/NiP-Fe:25% and RuO_2 for OER in alkaline seawater.

Table S2. The percentage of different valence of Ni in A-NiFeP/NiP-Fe:10%, A-NiFeP/NiP-Fe:25%, NiP.

Catalysts	Ni^0	Ni^{2+}	Ni^{3+}
A-NiFeP/NiP-Fe:10%	6.3%	53.8%	39.9%
A-NiFeP/NiP-Fe:25%	3.0%	53.8%	43.2%
NiP	22.3%	32.7%	45.0%

Table S3. The percentage of different valence of Fe in A-NiFeP/NiP-Fe:10%, A-NiFeP/NiP-Fe:25%, FeP.

Catalysts	Fe^{0}	Fe^{2+}	Fe^{3+}
A-NiFeP/NiP-Fe:10%	26.4%	37.0%	36.6%
A-NiFeP/NiP-Fe:25%	32.8%	33.2%	34.0%
FeP	26.5%	47.7%	25.8%

Table S4. Comparison of the OER performances for A-NiFeP/NiP-Fe:25% with other previously reported electrocatalyst in 1 M KOH.

Catalysts	Tafel slope (mV dec^{-1})	η(mV)/ 10mA cm^{-2}	Refs.
A-NiFeP/NiP-Fe:25%	**31.8**	**241**	This work
Mo-NiCoP	76.7	269	[1]
NiP/NiFeP/C	58	250	[2]
NiFeCoP	36.3	277	[3]
NiCoP@NC NA	70.5	305	[4]
a-CoMoPx/CF	50.0	305	[5]
$Ni_3S_2/NiP_x/NF$	51.6	265	[6]
$Ni_{0.85}Fe_{0.15}PS/NF$	34	251	[7]
$NiFe_2O_4$@(Ni,Fe)S/P	42	261	[8]
Fe-NiCoP	75.2	266	[9]

Table S5. Comparison of the HER performances for A-NiFeP/NiP-Fe:10% with other previously reported electrocatalyst in 1 M KOH.

Catalysts	Tafel slope (mV dec^{-1})	η(mV)/ 10mA cm^{-2}	Ref.
A-NiFeP/NiP-Fe:10%	**57.7**	**69.5**	This work
NiS/Ni_2P/CC	76.1	111	[10]
$Fe_{0.29}Co_{0.71}P$/NF	53.5	74	[11]
Ni_2P-$NiSe_2$/CC	65.7	89	[12]
Fe-Ni_5P_4/NiFeOH	94	197	[13]
Fe-Ni_2P/MoS_x/NF	59.7	112	[14]
Ni_2P/Ni_3S_2/NF	65	80	[15]
NiCoFeP/C	108	149	[16]
FeCo-P	89.9	131	[17]
NiFeP@NiP@NF	97.9	105	[18]

Table S6. Comparison of the overall splitting performances for A-NiFeP/NiP-Fe:10% // A-NiFeP/NiP-Fe:25% with other previously reported electrocatalyst in 1 M KOH.

Cathodic catalysts	Anodic catalysts	Current density /mA cm^{-2}	Voltages/V	Refs.
A-NiFeP/NiP-Fe:10%	**A-NiFeP/NiP-Fe:25%**	**10**	**1.54**	**This work**
NiFeP@NC/Ni_2P	NiFeP@NC/Ni_2P	10	1.57	[19]
Co_4Ni_1P NTs	Co_4Ni_1P NTs	10	1.59	[20]
DLD-FeCoP@CNT	DLD-FeCoP@CNT	10	1.67	[21]
Co_xP-Fe_2P/NF	Co_xP-Fe_2P/NF	10	1.61	[22]
Co_2P/CoNPC	Co_2P/CoNPC	10	1.64	[23]
$NiCo_2O_4$/Ni_2P	$NiCo_2O_4$/Ni_2P	10	1.59	[24]
Fe, Rh-Ni_2P/NF	Fe, Rh-Ni_2P/NF	10	1.62	[25]
CoP@FeCoP/NC	CoP@FeCoP/NC	10	1.68	[26]
FeP_2-NiP_2@PC	FeP_2-NiP_2@PC	10	1.70	[27]

References

1. J. Lin, Y. Yan, C. Li, X. Si, H. Wang, J. Qi, J. Cao, Z. Zhong, W. Fei and J. Feng, Bifunctional electrocatalysts based on Mo-doped NiCoP nanosheet arrays for overall water splitting, *Nano-micro lett.,* 2019, **11**, 1-11.
2. B. Weng, X. Wang, C. R. Grice, F. Xu and Y. Yan, A new metal-organic open framework enabling facile synthesis of carbon encapsulated transition metal phosphide/sulfide nanoparticle electrocatalysts, *J. Mater. Chem. A*, 2019, **7**, 7168-7178.
3. M. Zhou, Q. Sun, Y. Shen, Y. Ma, Z. Wang and C. Zhao, Fabrication of 3D microporous amorphous metallic phosphides for high-efficiency hydrogen evolution reaction, *Electrochim. Acta*, 2019, **306**, 651-659.
4. B. Cao, Y. Cheng, M. Hu, P. Jing, Z. Ma, B. Liu, R. Gao and J. Zhang, Efficient and durable 3D self-upported nitrogen-doped carbon-coupled nickel/cobalt phosphide electrodes: stoichiometric ratio regulated phase-and morphology-dependent overall water splitting performance, *Adv. Funct. Mater.*, 2019, **29**, 1906316.
5. H. Huang, A. Cho, S. Kim, H. Jun, A. Lee, J. W. Han and J. Lee, Structural design of amorphous $CoMoP_x$ with abundant active sites and synergistic catalysis effect for effective water splitting, *Adv. Funct. Mater.*, 2020, **30**, 2003889.
6. X. Wang, X. Yu, S. Wu, P. He, F. Qin, Y. Yao, J. Bai, G. Yuan and L. Ren, Crystalline-Amorphous Interface Coupling of Ni_3S_2/NiP_x/NF with Enhanced Activity and Stability for Electrocatalytic Oxygen Evolution, *ACS Appl. Mater. Interfaces*, 2023, **15**, 15533-15544.
7. W. Peng, J. Li, K. Shen, L. Zheng, H. Tang, Y. Gong, J. Zhou, N. Chen, S. Zhao and M. Chen, Iron-regulated NiPS for enhanced oxygen evolution efficiency, *J. Mater. Chem. A*, 2020, **8**, 23580-23589.
8. Y.-L. Wang, T.-H. Yang, S. Yue, H.-B. Zheng, X.-P. Liu, P.-Z. Gao, H. Qin and H.-N. Xiao, Effects of Alternating Magnetic Fields on the OER of Heterogeneous Core-Shell Structured $NiFe_2O_4$@(Ni, Fe)S/P, *ACS Appl. Mater. Interfaces*, 2023, **15**, 11631-11641.
9. Y. Liu, P. Ge, Y. Li, X. Zhai, K. Lu, X. Chen, J. Yang, Z. Wang, H. Zhang and G. Ge, Prussian blue analogues derived Fe-NiCoP reveals the cooperation of Fe doping and phosphating for enhancing OER activity, *Appl. Surf. Sci.*, 2023, **615**, 156378.
10. X. Xiao, D. Huang, Y. Fu, M. Wen, X. Jiang, X. Lv, M. Li, L. Gao, S. Liu and M. Wang, Engineering NiS/Ni_2P heterostructures for efficient electrocatalytic water splitting, *ACS Appl. Mater. Interfaces*, 2018, **10**, 4689-4696.
11. H. Feng, L. Tang, G. Zeng, J. Yu, Y. Deng, Y. Zhou, J. Wang, C. Feng, T. Luo and B. Shao, Electron density modulation of $Fe_{1-x}Co_xP$ nanosheet arrays by iron incorporation for highly efficient water splitting, *Nano Energy*, 2020, **67**, 104174.
12. L. Yang, L. Huang, Y. Yao and L. Jiao, In-situ construction of lattice-matching $NiP_2/NiSe_2$ heterointerfaces with electron redistribution for boosting overall water splitting, *Appl. Catal. B Environ.*, 2021, **282**, 119584.
13. C.-F. Li, J.-W. Zhao, L.-J. Xie, J.-Q. Wu and G.-R. Li, Fe doping and oxygen vacancy modulated Fe-Ni_5P_4/NiFeOH nanosheets as bifunctional electrocatalysts for efficient overall water splitting, *Appl. Catal. B Environ.*, 2021, **291**, 119987.
14. X. Zhang, C. Liang, X. Qu, Y. Ren, J. Yin, W. Wang, M. Yang, W. Huang and X. Dong, Sandwich-Structured Fe-Ni_2P/MoS_x/NF Bifunctional Electrocatalyst for Overall Water Splitting, *Adv. Mater. Interfaces*, 2020, **7**, 1901926.
15. L. Zeng, K. Sun, X. Wang, Y. Liu, Y. Pan, Z. Liu, D. Cao, Y. Song, S. Liu and C. Liu, Three-dimensional-networked Ni_2P/Ni_3S_2 heteronanoflake arrays for highly enhanced electrochemical overall-water-splitting activity, *Nano Energy*, 2018, **51**, 26-36.
16. X. Wei, Y. Zhang, H. He, L. Peng, S. Xiao, S. Yao and P. Xiao, Carbon-incorporated porous honeycomb NiCoFe phosphide nanospheres derived from a MOF precursor for overall water splitting, *Chem. Commun.*, 2019, **55**, 10896-10899.

17. H. Jiang, Z. Zhao, G. Li, M. Wang, P. Chen, X. Liu, X. Tu, Y. Hu, Z. Shen and Y. Wu, Hollow Spherical Heterostructured FeCo-P Catalysts Derived from MOF-74 for Efficient Overall Water Splitting, *Adv. Sci.*, 2023, **11**, 2306919.
18. F. Diao, W. Huang, G. Ctistis, H. Wackerbarth, Y. Yang, P. Si, J. Zhang, X. Xiao and C. Engelbrekt, Bifunctional and self-supported NiFeP-layer-coated NiP rods for electrochemical water splitting in alkaline solution, *ACS Appl. Mater. Interfaces*, 2021, **13**, 23702-23713.
19. Q. Quan, Z. Lai, Y. Bao, X. Bu, Y. Meng, W. Wang, T. Takahashi, T. Hosomi, K. Nagashima and T. Yanagida, Self-Anti-Stacking 2D Metal Phosphide Loop-Sheet Heterostructures by Edge-Topological Regulation for Highly Efficient Water Oxidation, *Small*, 2021, **17**, 2006860.
20. L. Yan, L. Cao, P. Dai, X. Gu, D. Liu, L. Li, Y. Wang and X. Zhao, Metal-organic frameworks derived nanotube of nickel-cobalt bimetal phosphides as highly efficient electrocatalysts for overall water splitting, *Adv. Funct. Mater.*, 2017, **27**, 1703455.
21. B. Wang, Y. Chen, Q. Wu, Y. Lu, X. Zhang, X. Wang, B. Yu, D. Yang and W. Zhang, A co-coordination strategy to realize janus-type bimetallic phosphide as highly efficient and durable bifunctional catalyst for water splitting, *J. Mater. Sci. Technol.*, 2021, **74**, 11-20.
22. D. Li, C. Zhou, R. Yang, Y. Xing, S. Xu, D. Jiang, D. Tian and W. Shi, Interfacial Engineering of the Co_xP-Fe_2P Heterostructure for Efficient and Robust Electrochemical Overall Water Splitting, *ACS Sustain. Chem. Eng.*, 2021, **9**, 7737-7748.
23. H. Liu, J. Guan, S. Yang, Y. Yu, R. Shao, Z. Zhang, M. Dou, F. Wang and Q. Xu, Metal-Organic-Framework-Derived Co_2P Nanoparticle/Multi-Doped Porous Carbon as a Trifunctional Electrocatalyst, *Adv. Mater.*, 2020, **32**, 2003649.
24. L. Wang, C. Gu, X. Ge, J. Zhang, H. Zhu and J. Tu, Anchoring Ni_2P sheets on $NiCo_2O_4$ nanocone arrays as optimized bifunctional electrocatalyst for water splitting, *Adv. Mater. Interfaces*, 2017, **4**, 1700481.
25. M.-T. Chen, J.-J. Duan, J.-J. Feng, L.-P. Mei, Y. Jiao, L. Zhang and A.-J. Wang, Iron, rhodium-codoped Ni_2P nanosheets arrays supported on nickel foam as an efficient bifunctional electrocatalyst for overall water splitting, *J. Colloid Interface Sci.*, 2022, **605**, 888-896.
26. J. Shi, F. Qiu, W. Yuan, M. Guo and Z.-H. Lu, Nitrogen-doped carbon-decorated yolk-shell CoP@ FeCoP micro-polyhedra derived from MOF for efficient overall water splitting, *Chem. Eng. J.*, 2021, **403**, 126312.
27. P. Ji, H. Jin, H. Xia, X. Luo, J. Zhu, Z. Pu and S. Mu, Double metal diphosphide pair nanocages coupled with P-doped carbon for accelerated oxygen and hydrogen evolution kinetics, *ACS Appl. Mater. Interfaces*, 2019, **12**, 727-733.